Catalysis Today xxx (2013) xxx–xxx

Contents lists available at ScienceDirect

Catalysis Today

journal homepage: www.elsevier.com/locate/cattod

Dioxygen activation at room temperature during controllable and highly efficient acetaldehyde-to-acetic acid oxidation using a simple iron(III)–acetonitrile complex

Renhong Li [a], Hisayoshi Kobayashi [b,*], Xiaoqing Yan [a], Jie Fan [b,*]

[a] Key Lab of Applied Chemistry of Zhejiang Province, Department of Chemistry, Zhejiang University, Hangzhou, Zhejiang Province 310027, China
[b] Department of Chemistry and Materials Technology, Kyoto Institute of Technology, Matsugasaki, Sakyo-ku, Kyoto, Japan

ARTICLE INFO

Article history:
Received 26 June 2013
Received in revised form
10 September 2013
Accepted 16 September 2013
Available online xxx

Keywords:
Dioxygen activation
Iron–oxygen complex
Acetaldehyde oxidation
Michaelis–Menten kinetics

ABSTRACT

We show that highly efficient acetaldehyde-to-acetic acid oxidation is achieved in a diluted $FeCl_3$–acetonitrile solution (5–100 μM), which proceeds rather rapidly and follows the enzymatic-like Michaelis–Menten kinetics. Interestingly, by adjusting the concentration of $FeCl_3$, we are able to accelerate or shut down the oxidation process conveniently. Based on the catalytic results, spectroscopic evidences and successive DFT calculations, a reactant-initiated, putative mononuclear non-heme iron–oxygen complex, $[FeCl(MeCN)_4(O)]^{2+}$, is proposed as the active oxidizing species to conduct the room temperature reaction with relatively high TOF values (~1.2 s^{-1}). Finally, the putative iron–oxygen complexes are employed to the selective oxidation of benzyl alcohol under ambient conditions.

1. Introduction

Acetaldehyde (AcH) is an important industrial raw material, but also a common volatile organic compound and a probable carcinogen in humans. To oxidize AcH into non-hazardous acetic acid (AcOH) using dioxygen as the primary oxidant under ambient conditions is obviously beneficial for both industrial processes and public health. In human liver, AcH dehydrogenases catalyze the conversion of AcH into AcOH; this enzymatic process is known to prevent humans from many hangover symptoms [1]. However, as compared with natural dehydrogenases, so far few artificially synthesized catalysts have been explored for such efficient transformation with turnover frequency (TOF) up to a few molecules per catalytic center per second at room temperature (~25 °C).

To make a successful AcH-to-AcOH conversion, the participant catalysts should be able to activate molecular dioxygen at low temperatures. Mononuclear non-heme iron enzymes are of this type. For these kind of enzymes, the high-valent Fe(IV)-oxo intermediates have been experimentally and theoretically demonstrated to be the active oxidizing species [2–7]. In order to mimic natural enzymes and to enhance the substrate reactivity of mononuclear nonheme oxoiron(IV) intermediates, usually artificial oxidants, complicated supporting ligands, and/or cofactors are essential. Therefore, it is of fundamental scientific and practical importance to employ pristine ligands (e.g. acetonitrile, MeCN) plus dioxygen as the terminal oxidant to construct synthetic iron–oxygen species for biomimetic reactions. Herein, we report oxidative dehydrogenation of AcH to AcOH can be rapidly accomplished in a homogenous system containing only micromole level $FeCl_3$ and MeCN solvent at room temperature. Interestingly, the reaction is found to follow the Michaelis–Menten kinetics, suggesting its probable enzymatic-like catalytic nature. Furthermore, by simply adjusting the concentration of $FeCl_3$, we are able to expediently accelerate or turnoff the oxidation reaction, making the whole process to be controllable. Based on the catalytic results, spectroscopic evidences and DFT calculations, a reactant-initiated, putative mononuclear non-heme iron–oxygen complex, $[FeCl(MeCN)_4(O)]^{2+}$, is proposed as the active oxidizing species to conduct the room temperature reaction with TOF values (~1.2 s^{-1}) comparable to that of natural aldehyde dehydrogenases.

2. Experimental

2.1. Catalysis part

Aerobic AcH oxidation experiments were carried out in a quartz tube containing different amount of $FeCl_3$ in CH_3CN (5 mL) in air at

* Corresponding authors. Tel.: +86 571 86843624; fax: +86 571 86843624.
E-mail addresses: kobayashi@chem.kit.ac.jp (H. Kobayashi), jfan@zju.edu.cn (J. Fan).

0920-5861/$ – see front matter © 2013 Elsevier B.V. All rights reserved.
http://dx.doi.org/10.1016/j.cattod.2013.09.036

room temperature. The AcH and products concentrations were calculated from the results of GC-FID analysis, and then calculated the substrate conversion and the selectivity toward AcH (benzene was used as an external standard). GC-TCD was employed for determination of the gas-phase products. The conditions for benzyl alcohol oxidation were similar to the above AcH oxidation process, except that benzyl alcohol (0.02 M) was added into the solution containing different amount of AcH, $FeCl_3$ in CH_3CN (5 mL). The substrate conversion and the selectivity toward benzaldehyde (toluene was used as an external standard) were calculated from the results of GC-FID and GC-TCD analysis.

2.2. Spectroscopic studies

Accurate mass spectrometry data were obtained using Apex III (7.0 Tesla) Fourier transform ion cyclotron resonance tandem mass spectrometry (FTICR-MS/MS) (Bruker, Billerica, MA, USA), equipped with XMASS software (Bruker, version 6.1.1) used for instrument control, data acquisition and processing. Sodium trifluoroacetate was used as an external calibration compound. Solutions were infused from the ESI source at 3 mL/min with the following parameters applied: capillary, −4771 V; end plate, −4413 V; skimmer 1, 12.00 V; skimmer 2, 6.61 V; offset, 0.98 V; RF amplitude, 582.5 Hz; drying gas temperature, 150 °C. Nitrogen was used as the nebulizing and drying gas and argon was used as the collision gas. X-band EPR signals were recorded at ambient temperature on a Bruker EPR A-300 spectrometer. The settings for the EPR spectrometer were as follows: center field, 3511.39 G; sweep width, 100 G; microwave frequency, 9.86 G; modulation frequency, 100 kHz; power, 101 mW; conversion time, 10 ms. A glass capillary tube containing calculated $FeCl_3$, AcH and acetonitrile solution, and ice-cooled DMPO solution (0.08 M) was transferred and tested by EPR spectroscopy at room temperature. No signals are observed in the following systems: (1) $FeCl_3$, AcH and CH_3CN in the absence of DMPO, (2) $FeCl_3$, DMPO and MeCN, (3) DMPO, MeCN and AcH in open air, and (4) DMPO, CH_3CN, and other organic substrates (e.g. HCHO, MeOH, and AcOH) were employed.

2.3. Outline of DFT calculation

The hybrid type density functional theory method so-called the Becke three-parameter Lee–Yang–Parr functional was employed [8–11]. The Los Alamos effective core potential was used for the Fe atom [12], and the 3s, 3p 3d, and 4s electrons of Fe and all the electrons for the first row atoms were dealt with the valence double quality basis sets [13] which are implemented in the Gaussian 03W package [14]. The reactions were simulated in vacuum. However, a part of calculation was carried out including the solvation effects employing the self consistent reaction field theory at the level of polarizable continuum model.

The whole reaction is divided into four elementary steps. There are four transition states (TS's). First TS is characterized, and then the intrinsic reaction coordinate (IRC) is evaluated to both directions [15–17]. From each end point of the IRC, usual geometry optimization leads to the reactant or product as the local minimum.

3. Results and discussion

By accident, we found that AcH can be efficiently oxidized into AcOH in a homogeneous system containing micromole level $FeCl_3$ and MeCN solvent at room temperature (25 °C), while negligible reaction occurred under the following conditions: (i) in the absence of $FeCl_3$ or other instead iron salts (e.g. $FeSO_4$, $Fe_2(SO_4)_3$, and $Fe(NO_3)_3$) were used, (ii) MeCN solvent was replaced by THF, CH_2Cl_2 or H_2O, and (iii) other analogous metal chlorides (e.g. $ZnCl_2$, $CoCl_2$, $RuCl_3$, and $MnCl_2$) were used as the catalysts. The parallel experiments demonstrate that the auto-oxidation of AcH into AcOH is not possible at low temperatures, and they also indicate that the combination of $FeCl_3$ and MeCN is unique to the AcH oxidation process. The conversion, selectivity, and TOF value of aerobic oxidation of AcH (0.08 M) into AcOH with a broad range of $FeCl_3$ concentration are summarized in Table 1. When the concentration of $FeCl_3$ (abbreviated as [**$FeCl_3$**]) is less than 1.0 μM, no obvious transformation of AcH is observed after 2 h reaction (entry 2, Table 1). Increasing the [**$FeCl_3$**] has a prominent impact on the conversion of AcH: more than 70% of AcH is oxidized within 1 h when 100 μM $FeCl_3$ (0.5 μmol) was employed (entry 7, Table 1), while 2 h reaction only enables 7.8% AcH to be oxidized as [**$FeCl_3$**] was further increased to 20 mM (200-fold) (entry 10, Table 1). Notably, the TOF values increased significantly with increasing [**$FeCl_3$**] to a maximum (1.21 s^{-1}, entry 5, Table 1) at ca. 10 μM, with the value dropping gradually at higher content.

Table 1
AcH (0.08 M) oxidation into AcOH over $FeCl_3$ with a variety of concentration in CH_3CN solvent at room temperature (25 °C).

Entry	[$FeCl_3$][a]	t/min	Conv./%[b]	Sel./%[c]	TOF/s^{-1}
1	0	120	0	–	0
2	1.0	120	0	–	0
3	2.5	120	2.1	>99	0.09
4	5.0	120	36.8	92	0.82
5	10	60	54.4	88	1.21
6	20	60	43.4	85	0.48
7	100	60	73.8	84	0.16
8	200	140	74.5	80	0.035
9	2×10^3	140	16.1	75	8×10^{-4}
10	2×10^4	120	7.8	65	4.4×10^{-5}

[a] $FeCl_3$ concentration in CH_3CN.
[b] The conversion is based on the results of GC analysis.
[c] During AcH to AcOH oxidation, formaldehyde, formic acid, CO_2, etc. were formed as by-products, which results in the decrease of selectivity upon elongated reaction.

In order to understand the reaction dynamics more clearly, the TOF variation as a function of [**$FeCl_3$**] in logarithm is shown in Fig. 1a. It is noteworthy that the TOF distribution is nearly Gaussian-shaped (red parabolic curve), peaking at $\ln[\mathbf{FeCl_3}] \approx 2.0$. The above results suggest that the initial concentration of $FeCl_3$ largely affects the AcH-to-AcOH transformation, making the whole process to be controllable. Such a catalyst-concentration-dependent catalytic process is rare and interesting, implying that unique catalytic centers may be formed in such a diluted concentration range (5–100 μM) similar to previous observation of active gold cluster for CO oxidation [18].

The kinetics of AcH oxidation was further analyzed by varying the concentration of AcH (abbreviated as [**AcH**]) with [**$FeCl_3$**] at a given value of 20 μM (0.1 μmol). As shown in Table 2, only limited conversion is observed when [**AcH**] below 0.02 M (entry 1, Table 2), but it is intriguing to note that the conversion rate speeds up upon increasing [**AcH**] and reaches an optimal concentration at 0.2 M (entry 6, Table 2). By plotting the TOF data against [**AcH**], we

Table 2
The oxidation of AcH with concentration from 0.02–1.0 M over $FeCl_3$ (20 μM) in CH_3CN at room temperature.

Entry	[AcH][a]	t/min	Conv./%	Sel./%	TOF/s^{-1}
1	0.02	30	0.9	>99	0.016
2	0.04	60	12.9	87	0.072
3	0.08	30	13.2	86	0.294
4	0.12	30	12.1	94	0.601
5	0.16	30	22.7	89	1.01
6	0.2	30	22.9	89	1.27
7	0.4	30	12.9	95	1.43
8	0.8	30	7.5	94	1.66
9	1.0	30	6.3	96	1.75

[a] AcH concentration.

Please cite this article in press as: R. Li, et al., Dioxygen activation at room temperature during controllable and highly efficient acetaldehyde-to-acetic acid oxidation using a simple iron(III)–acetonitrile complex, Catal. Today (2013), http://dx.doi.org/10.1016/j.cattod.2013.09.036

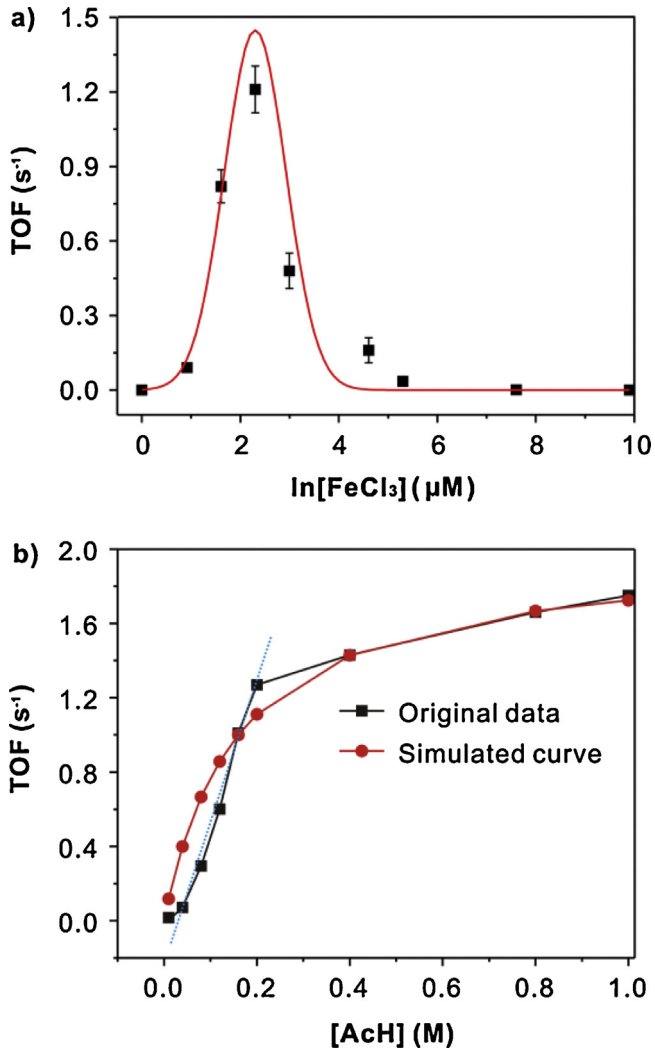

Fig. 1. (a) The TOF variation as a function of the concentrations of $FeCl_3$ in logarithm during AcH (0.08 M) oxidation in MeCN, and (b) plots of the TOF data against the concentrations of AcH using 20 μM $FeCl_3$ as catalyst in MeCN (black line). (For interpretation of the references to colour in this figure legend, the reader is referred to the web version of this article.)

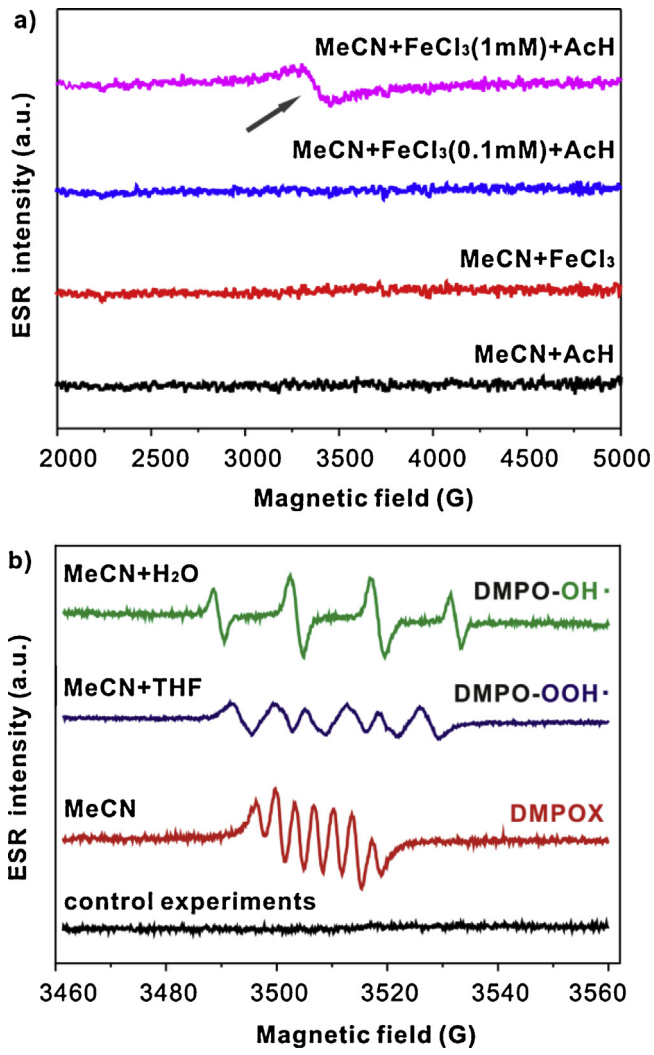

Fig. 2. (a) ESR spectra of various $FeCl_3$-involving systems, and (b) DMPO spin trapping adducts recorded in the AcH/$FeCl_3$/MeCN system ([**$FeCl_3$**] = 1 mM) with/without co-solvent at room temperature.

noticed that the catalytic reaction obeys the first order reaction at the initial stage (as simulated by the dashed line), and then exhibits a pseudo zero order reaction at high [**AcH**] (Fig. 1b). The substrate concentration-dependent catalytic process has been well established in biochemical reactions, for example, Michaelis–Menten model [19]. This model takes the form of an equation describing the rate of enzymatic reactions, by relating reaction rate ***R*** to [**S**] (**S** = substrate):

$$\mathbf{R} = V_{\max}[\mathbf{S}]/(K_{\mathrm{m}} + [\mathbf{S}]) \quad (1)$$

where $V_{\max}$ represents the maximum rate achieved by the system at maximum substrate concentrations, and K_{m} the Michaelis constant. Considering that (i) high TOF values (up to 2.0 s^{-1}) are not always observed in normal catalytic systems carried out at room temperature, and (ii) the apparent activation energy of this chemical reaction is as low as 39.3 kJ mol^{-1} (Figure S1), we assume that the AcH aerobic oxidation in $FeCl_3$/MeCN system resembles an enzymatic process that follows the Michaelis–Menten kinetics. By analyzing the trend of the present catalytic process, we set parameter $V_{\max}$ as 2.0 s^{-1}. Parameter K_{m} is then calculated to be 0.16 M according to the first order reaction equation:

$$\mathbf{TOF} = 7.78[\mathbf{AcH}] - 0.28 \quad (2)$$

Therefore, for AcH oxidation in $FeCl_3$/MeCN system at room temperature, its analogous Michaelis–Menten equation is simplified to:

$$\mathbf{TOF} = 2[\mathbf{AcH}]/(0.16 + [\mathbf{AcH}]) \quad (3)$$

Fig. 1b shows that the curve simulated by Eq. (3) (red line) fits properly with the experimental data.

The above experimental observations strongly imply that enzymatic-like iron–oxygen species responsible for efficient AcH oxidation may be generated. Therefore room temperature electron spin resonance (ESR) spectroscopy and spin trapping technique were employed to detect possible catalytic species. As shown in Fig. 2a, no observable signals were found neither in the $FeCl_3$/MeCN binary system with [**$FeCl_3$**] ranging from 0.1 to 10 mM, nor in the AcH/$FeCl_3$/MeCN ternary system with [**$FeCl_3$**] = 0.1 mM. However, as [**$FeCl_3$**] increased to 1 mM, a Lorentzian signal (black arrow) appeared which may be ascribed mainly to the Fe^{3+} cluster coupled by strong spin–spin interaction. The present signal is located around g = 1.994, which is close to the free electron value of g_e = 2.00372 corresponding to the symmetrical tetrahedral

Please cite this article in press as: R. Li, et al., Dioxygen activation at room temperature during controllable and highly efficient acetaldehyde-to-acetic acid oxidation using a simple iron(III)–acetonitrile complex, Catal. Today (2013), http://dx.doi.org/10.1016/j.cattod.2013.09.036

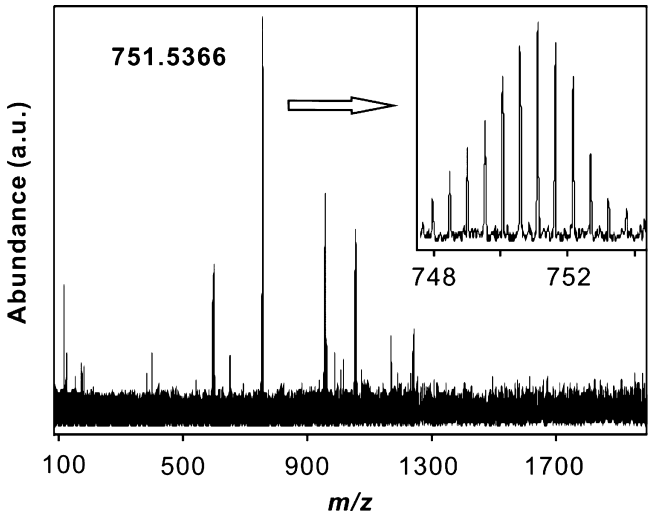

Fig. 3. ESI MS spectrum of AcH/$FeCl_3$/MeCN ternary system using HPLC-grade MeCN as the solvent; inset shows the isotope distribution patterns of the ion at m/z = 751.5366.

isolated Fe^{3+} ions, coupled by strong dipolar and superexchange interactions [20]. It has been reported that the ESR may arise from σ-electron radicals, exhibiting g-factor < g_e. Thus these unpaired electrons are expected to be captured by dioxygen at room temperature to afford iron–oxygen species at a given [**$FeCl_3$**]. The spin trapping experiments further manifested this assumption. As shown in Fig. 2b, a seven-line signal (red line) designated to DMPOX (hyperfine splitting constants: α_N = 6.98 G and α_H = 3.81 G) immediately appeared by addition of AcH into the $FeCl_3$/MeCN system [21], whereas no signals were detected in the control experiments (black line, see Section 2 for details). The formation of DMPOX adduct is potentially ascribed to the oxidation of DMPO by high valent Fe(IV)═O oxidizing species. Interestingly, the ESR signals are largely influenced by co-solvent: a six-line signal corresponding to DMPO—OOH• adduct (α_N = 13.2 G, α_H^{β} = 8.5 G, and α_H^{γ} = 1.8 G), and a quadruple DMPO—OH• adduct ($\alpha_N = \alpha_H$ = 14.2 G) are observed when THF (blue line) and water (green line) were used as co-solvents, respectively. The origin of the co-solvent dependent character for the ESR signals is unclear at this moment [22], yet at least these signals indicate that various iron–oxygen species are present in the AcH/$FeCl_3$/MeCN ternary system.

The electrospray ionization mass spectrum (ESI MS) is a powerful tool to verify possible ions in liquid phase, thus it was employed for further detecting any iron–oxygen ions present in the ternary AcH/$FeCl_3$/MeCN system. In this case, a prominent ion at a mass-to-charge ratio (m/z) of 751.5366 is observed, whose mass and isotope distribution pattern correspond to a putative adduct of $[FeCl(O)(MeCN)_{19}]^{2+}$ (calculated m/z = 751.5331) (Fig. 3). Although the direct interaction between abundant additional solvent molecules and iron–oxygen adducts is uncommon in ESI MS studies, it may be relative to the fact that MeCN not only serves as supporting ligands but also solvent in the present work. On the other hand, it has been reported that MeCN is able to form even pentamers via hydrogen bonding interaction [23]. If this was true, it is possible that $[FeCl(MeCN)_4(O)]^{2+}$ ion interacts with merely three MeCN pentamers to stabilize itself during ESI MS sampling and thus affords the observed ion. In addition, it is noted that the presence of AcOH has negligible effect on the catalytic properties of the $FeCl_3$–MeCN complex. Further, we also carried out DFT calculation to compare the binding energies of AcOH and MeCN using $Fe(MeCN)_4Cl$ complex in the quartet and sextet. It reveals that the binding energy is larger for MeCN both in the quartet and sextet. Therefore, the $FeCl_3$–MeCN complex is not easy to decompose even in the presence of AcOH, and we expect that this complex is a relatively stable catalytic system.

To elucidate the reaction pathways and mechanisms, as well as possible active oxidizing species, DFT calculations were performed using Gaussian03W software together with the B3LYP functional and LanL2DZ basis set (see supporting information for details). Before doing so, considering the previous ESR and ESI MS results, it is highly possible that $FeCl_3$ interacts with MeCN to produce a complex serving as the real oxidizing catalyst. This is rather true since MeCN has long been demonstrated to be not only favorable electron donor solvent, but also promising ligand to $FeCl_3$ as described in Eq. (4) [24].

$$2FeCl_3 + 4MeCN \rightarrow [FeCl_2(MeCN)_4]^+ + [FeCl_4]^- \quad (4)$$

Between the two complexes in the right hand side of Eq. (4), $[FeCl_2(MeCN)_4]^+$ is thought to be the precursor of active catalyst which oxidizes AcH into AcOH (Figure S2 and S3, see supporting information). However, for the coordination of O_2 molecule, either Cl^- or MeCN ligand must be detached, and five coordinated $[FeCl_2(MeCN)_3]^+$ or $[FeCl(MeCN)_4]^{2+}$ is considered as the real catalyst species (Figure S4 and S5, see supporting information). The whole reaction is decomposed into four elementary reactions as shown below:

$$[FeCl_{5-n}L_nO_2]^{(n-2)+} + AcH \rightarrow [FeCl_{5-n}L_nOOH]^{(n-2)+} + Ac^{\bullet} \quad (5)$$

$$[FeCl_{5-n}L_nOOH]^{(n-2)+} + Ac^{\bullet} \rightarrow [FeCl_{5-n}L_nO]^{(n-2)+} + AcOH \quad (6)$$

$$[FeCl_{5-n}L_nO]^{(n-2)+} + AcH \rightarrow [FeCl_{5-n}L_nOH]^{(n-2)+} + Ac^{\bullet} \quad (7)$$

$$[FeCl_{5-n}L_nOH]^{(n-2)+} + Ac^{\bullet} \rightarrow [FeCl_{5-n}L_n]^{(n-2)+} + AcOH \quad (8)$$

where n represents 4 or 3, and MeCN is abbreviated by L. In each reaction, the transition state (TS) was characterized first, which was confirmed by the harmonic frequency analysis. The intrinsic reaction coordinate (IRC) analysis and successive optimization were carried out to both directions, i.e. the reactant and product sides. However, for example, the product of Eq. (5) and the reactant of Eq. (6) are not completely the same structure due to the change of mutual orientation.

Fig. 4 shows the order of spin states and the structures of $[FeCl(MeCN)_4(O_2)]^{2+}$ complex. The ground state is the quartet state, which is understood by the antiparallel coupling between the sextet $[FeCl(MeCN)_4]^{2+}$ complex and the triplet O_2 molecule. The almost degenerate octet state is a consequence of parallel coupling between the sextet complex and the O_2 molecule. The O—O distance in coordinated O_2 is 1.26 to 1.27 Å, which is only slightly elongated than the value of free molecule (1.207 Å). It means that the O_2 molecule is not so activated even coordinated to the Fe complex. The intermediate spin coupling sextet state is higher than the both spin states. Similar discussion with $[FeCl_4(O_2)]^-$ complex is shown in Figure S6 (supporting information); the long Fe—O_2 distances and the slightly lengthened O—O bond suggest the weak interaction between $[FeCl_4]^-$ and O_2.

In the following, the sum of energies of isolated Fe complex ($[FeCl(MeCN)_4]^{2+}$ or $[FeCl_2(MeCN)_3]^+$), O_2 and two AcH molecules is adopted as the zero of relative energy. The energy and structural changes along the elementary reactions (5) to (8) are shown in Figure S7 to S10 (supporting information) for $[FeCl(MeCN)_4]^{2+}$, and Figure S12 to S15 (supporting information) for $[FeCl_2(MeCN)_3]^+$. Fig. 5 summarizes the energy change along the whole reaction, in which four TS's are labeled as TS1 to TS4, corresponding to Eqs. (5) to (8).

The two Fe complexes gave relatively similar energetics (black and purple line in Fig. 5), and the results with $[FeCl_2(MeCN)_3]^+$ are referred in the supporting information to avoid redundancy.

Please cite this article in press as: R. Li, et al., Dioxygen activation at room temperature during controllable and highly efficient acetaldehyde-to-acetic acid oxidation using a simple iron(III)–acetonitrile complex, Catal. Today (2013), http://dx.doi.org/10.1016/j.cattod.2013.09.036

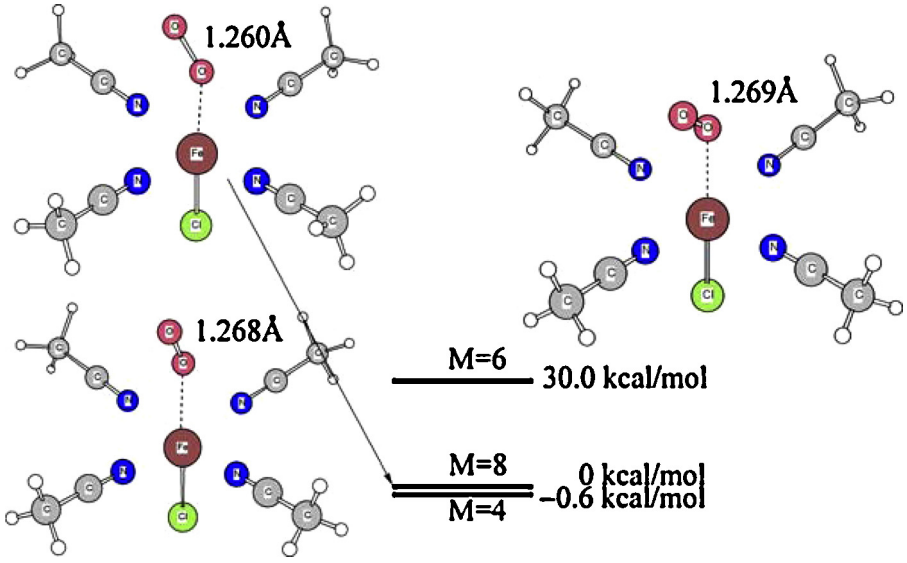

Fig. 4. Optimized structure and spin states for $[FeCl(MeCN)_4(O_2)]^{2+}$ complex.

TS1 is the TS for the C—H bond fission and the activation energy of 16.3 kcal mol^{-1} is the highest energy in the overall reaction. The products are $[FeCl(MeCN)_4OOH]^{2+}$ and Ac• radical (LM2), which are connected by the hydrogen bonding. We also searched other reaction mechanisms: (i) the O—O bond dissociates first and the O atom inserts into the C—H bond of AcH, or (ii) the H atom migrates from the C—H bond to form the O—H bond, and simultaneously the O—O bond dissociates and the O atom bonds to the C atom. However, such TS's could not be obtained at all.

The product of Eq. (5) is not so stable (+1.2 kcal mol^{-1}) but it is more stabilized by 19 kcal mol^{-1} by changing the orientation to the reactant of Eq. (6). The activation energy for Eq. (6) was 11.3 kcal mol^{-1} and the product is the Fe(IV)═O complex and AcOH molecule. Eq. (7) is the former half of the second oxidation between $[FeCl(MeCN)_4(O)]^{2+}$ and AcH. The TS for C—H bond fission (TS3) locates in very close to the reactant in the structure and energy. This small activation energy implies that the oxo complex is more active than $[FeCl(MeCN)_4(O_2)]^{2+}$. The resulting product is $[FeCl(MeCN)_4OH]^{2+}$ and Ac• radical. In the last elementary reaction Eq. (8), Ac• radical interacts with Fe(III)—OH. The activation energy for TS4 is 10 kcal mol^{-1} measured from the product of Eq. (7), or almost zero measured from the associated reactant structure. The Fe(III)—OH bond fission occurs easily, and the product stabilizes by ca. 31 kcal mol^{-1}. A large negative value of the relative energy is a result of enthalpy change for $2AcH + O_2 \rightarrow 2AcOH$, and the desorption energy for AcOH is only a few kcal mol^{-1}. Since solvation effects sometimes significantly change the energy barrier of TS, we also carried out single point calculations from LM1 through LM5 with solvation effects and with quartet spin state. The difference of energy profiles is shown in Fig. S16 (supporting information). In the former half, the two energy plots change in parallel except for LM2′, and in the latter half, the two energy plots are almost overlapped. The averaged destabilization energies are 19 and 6 kcal mol^{-1} for the former and latter half, respectively. The activation energies for TS's are changed by the solvation effects as follows: 16.3–18.1 kcal mol^{-1} for TS1, 13.4 to 27.4 kcal mol^{-1} for TS2, 0.0 to −0.6 kcal mol^{-1} for TS3, and 0.4–1.4 kcal mol^{-1} for TS4. Except for TS2, the change in energy is small. The abnormality of TS2 is caused by an excessive stabilization of LM2′. LM2′ with the solvation effects works like a small hollow on the potential energy surface, but the reaction proceeds similarly on both the potential energy surfaces.

The reason of destabilization with the solvation effects is explained. The sum of extra stabilization energies by the solvation effects is $-0.3 + (-5.8) + (-134.2)$ kcal mol^{-1} for the isolated (O_2 + AcH + FeL_4Cl) system, but −122.5 kcal mol^{-1} for LM1. This means that the solvation effects more stabilize the isolated system, and the upper plot line in Figure S16 is obtained in the former half. In the latter half, one AcOH molecule co-exists in the system, and its extra stabilization energy (−10.7 kcal mol^{-1}) is lower than that for AcH molecule (−5.8 kcal mol^{-1}). This partly diminishes the difference between the two plots.

Based on the DFT calculation and spectra data presented so far, there is strong circumstantial evidence, but not direct definitive proof, that high-valent mononuclear iron–oxygen complexes do exist in the ternary AcH/$FeCl_3$/MeCN system. To this end, considering the iron–oxygen complexes are well-known powerful oxidants that can cleavage and abstract H atoms from C—H bonds under ambient conditions [25], we expect that the iron–oxygen species may be useful for other organic substrates oxidation if they are present. Noting that the selective oxidation of alcohols is one of the most important transformations in organic synthesis [26], we performed catalytic aerobic oxidation of benzyl alcohol to benzaldehyde within the ternary AcH/$FeCl_3$/MeCN system at room

Table 3
Benzyl alcohol (0.02 M) selective oxidation to benzaldehyde in the ternary system containing $FeCl_3$, AcH, and CH_3CN (5 mL) in air at room temperature.[a]

Entry	[$FeCl_3$]/μM	t/h	[AcH]/M	Conv./%	Sel./%[b]	TOF/h^{-1}[c]
1	0	12	0.08	0	–	–
2	10	12	0	0	–	–
3	1	12	0.08	1.2	>99	1
4	10	12	0.08	77.4	98.7	12.9
5	20	12	0.08	74.9	98.2	6.2
6	100	12	0.08	75.4	95.3	1.3
7	200	12	0.08	80.2	90.4	0.7
8	10	12	0.01	1.5	>99	0.25
9	10	12	0.04	17	99	2.8
10	10	3	0.16	2.1	>99	14
11	10	3	0.32	3.0	>99	20

[a] Toluene is used as an external standard, and the products are determined by GC.
[b] Benzoic acid is produced as a by-product, which leads to the decrease of benzaldehyde selectivity.
[c] TOF values are calculated only for benzyl alcohol conversion on per molar $FeCl_3$ per hour; the AcH conversion is not included here.

Please cite this article in press as: R. Li, et al., Dioxygen activation at room temperature during controllable and highly efficient acetaldehyde-to-acetic acid oxidation using a simple iron(III)–acetonitrile complex, Catal. Today (2013), http://dx.doi.org/10.1016/j.cattod.2013.09.036

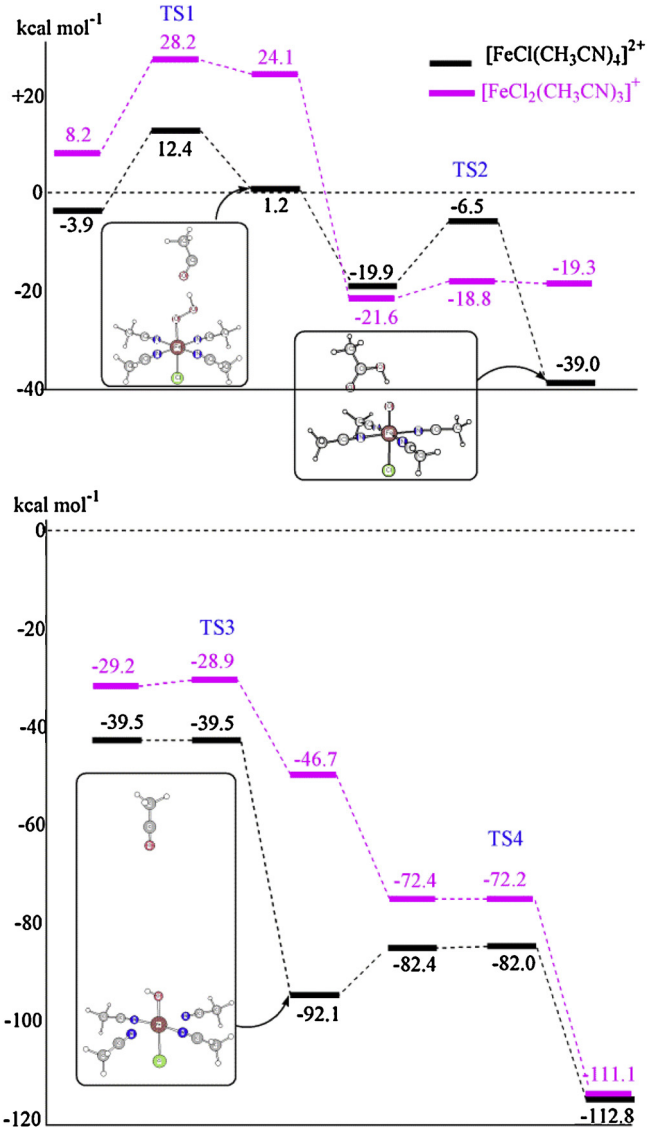

Fig. 5. The combined energy profile for overall reactions: two AcH molecules are oxidized into two AcOH molecules by $[FeCl(MeCN)_4]^{2+}$ (black) and $[FeCl_2(MeCN)_3]^{+}$ (purple) complexes with assistance of dioxygen. The former half corresponds to Eqs. (5) and (6), and the latter corresponds to Eqs. (7) and (8) of the reaction. The insets show the structures of Fe(III)—OOH + Ac·, Fe(IV)═O + AcOH, and Fe(III)—OH + Ac· intermediates generated during the catalytic reaction, and round arrows indicate their energy levels for the case of $[FeCl(MeCN)_4]^{2+}$. (For interpretation of the references to colour in this figure legend, the reader is referred to the web version of this article.)

temperature (Table 3). It is noteworthy that no benzyl alcohol conversion occurs in the absence of $FeCl_3$ or AcH (entries 1–2), while promising conversions are achieved with the increase of [**$FeCl_3$**] at [**AcH**] = 0.08 M (entries 4–7, Table 3). The optimal TOF value for the reaction reaches 20 h^{-1} when [**AcH**] increases to 0.32 M (entry 11, Table 3). For benzyl alcohol oxidation, the examples of such room temperature reactions using non-noble metals as the catalysts are rare [27,28]. We suppose that the high catalytic activities at low temperatures are derived from the strong oxidation capability of the iron–oxygen adducts. This in turn provides another proof of the existence of mononuclear iron–oxygen complexes in the simple AcH/$FeCl_3$/MeCN system, since the auto-oxidation of AcH to AcOH can stimulate the generation of this iron–oxygen complex.

4. Conclusions

In summary, we have reported the first example showing AcH undergoes rapid aerobic oxidation and proceeds in a controlled manner in a primitive $FeCl_3$/MeCN mixture at room temperature, which follows the typical Michaelis–Menten kinetics. On the basis of our experimental results and theoretical calculations, we propose that the reactant (AcH) initiates the room temperature dioxygen activation that leads to the generation of $[FeCl(MeCN)_4(O)]^{2+}$ oxidizing species for aldehydes-to-acid oxidation. We further applied these active complexes to the selective oxidation of benzyl alcohol under ambient conditions with promising TOF values. Finally, it is worth mentioning that prior to the commercialization of the Monsanto process – the carbonylation of methanol, most AcOH was produced from catalytic oxidation of AcH, which now remains the second-most important manufacturing method in industry. Thus the efficient oxidation of AcH to AcOH using earth-abundant iron-involved catalysts under ambient conditions is also attractive for industrial purposes.

Acknowledgments

Authors are grateful to M. Kobayashi, S. Morimoto, and K. Yamamoto in KIT for their computer operation and graphical drawings, and Prof. Y. Pan and C. Guo in ZJU for ESI MS analysis. This work was supported by the Grand-in-Aid of Japan (No. 23560934), the National Science Foundation of China (20873122, 21222307, and 21003106), Fok Ying Tung Education Foundation (131015), and the Fundamental Research Funds for the Central Universities (2012QNA3014).

Appendix A. Supplementary data

Supplementary data associated with this article can be found, in the online version, at http://dx.doi.org/10.1016/j.cattod.2013.09.036.

References

[1] R. Vallari, R. Pietruszko, Science 216 (1982) 637.
[2] L. Que, R.Y.N. Ho, Chem. Rev. 96 (1996) 2607.
[3] C. Krebs, D.G. Fujimori, C.T. Walsh, J.M. Bollinger, Acc. Chem. Res. 40 (2007) 484.
[4] J. Hohenberger, K. Ray, K. Meyer, Nat. Commun. 3 (2012) 720.
[5] W. Nam, Acc. Chem. Res. 40 (2007) 522.
[6] M. Costas, M.P. Mehn, M.P. Jensen, L. Que, Chem. Rev. 104 (2004) 939.
[7] M.M. Abu-Omar, A. Loaiza, N. Hontzeas, Chem. Rev. 105 (2005) 2227.
[8] A.D. Becke, Phys. Rev. A 38 (1988) 3098.
[9] C. Lee, W. Yang, R.G. Parr, Phys. Rev. B 37 (1988) 785.
[10] A.D. Becke, J. Chem. Phys. 98 (1993) 1372.
[11] P.M.W. Gill, B.G. Johnson, J.A. Pople, M.J. Frisch, J. Int, Quantum Chem. (1992) 319.
[12] P.J. Hay, W.R. Wadt, J. Chem. Phys. 82 (1985) 270.
[13] T.H.J. Dunning, P.J. Hay, in: H.F. Schaefer III (Ed.), Modern Theoretical Chemistry, Plenum Press, New York, 1976, pp. 1–35.
[14] M.J. Frisch, G.W. Trucks, H.B. Schlegel, G.E. Scuseria, M.A. Robb, J.R. Cheeseman, J.A. Montgomery Jr., T. Vreven, K.N. Kudin, J.C. Burant, J.M. Millam, S.S. Iyengar, J. Tomasi, V. Barone, B. Mennucci, M. Cossi, G. Scalmani, N. Rega, G.A. Petersson, H. Nakatsuji, M. Hada, M. Ehara, K. Toyota, R. Fukuda, J. Hasegawa, M. Ishida, T. Nakajima, Y. Honda, O. Kitao, H. Nakai, M. Klene, X. Li, J.E. Knox, H.P. Hratchian, J.B. Cross, C. Adamo, J. Jaramillo, R. Gomperts, R.E. Stratmann, O. Yazyev, A.J. Austin, R. Cammi, C. Pomelli, J.W. Ochterski, P.Y. Ayala, K. Morokuma, G.A. Voth, P. Salvador, J.J. Dannenberg, V.G. Zakrzewski, S. Dapprich, A.D. Daniels, M.C. Strain, O. Farkas, D.K. Malick, A.D. Rabuck, K. Raghavachari, J.B. Foresman, J.V. Ortiz, Q. Cui, A.G. Baboul, S. Clifford, J. Cioslowski, B.B. Stefanov, G. Liu, A. Liashenko, P. Piskorz, I. Komaromi, R.L. Martin, D.J. Fox, T. Keith, M.A. Al-Laham, C.Y. Peng, A. Nanayakkara, M. Challacombe, P.M.W. Gill, B. Johnson, W. Chen, M.W. Wong, C. Gonzalez, J.A. Pople, Gaussian 03, Revision B.03, Gaussian Inc., Pittsburgh, PA, 2003.
[15] K. Fukui, Acc. Chem. Res. 14 (1981) 363.
[16] C. Gonzalez, H.B. Schlegel, J. Chem. Phys. 90 (1989) 2154.
[17] C. Gonzalez, H.B. Schlegel, J. Phys. Chem. 94 (1990) 5523.
[18] M.S. Chen, D.W. Goodman, Science 306 (2004) 252.
[19] K.A. Johnson, R.S. Goody, Biochemistry 50 (2011) 8264.
[20] E.M. Abdelrazek, Phys. B – Condens. Matter 400 (2007) 26.

[21] R. Li, H. Kobayashi, J. Tong, X. Yan, Y. Tang, S. Zou, J. Jin, W. Yi, J. Fan, J. Am. Chem. Soc. 134 (2012) 18286.
[22] S. Hong, Y.M. Lee, W. Shin, S. Fukuzumi, W. Nam, J. Am. Chem. Soc. 131 (2009) 13910.
[23] B. Kharat, V. Deshmukh, A. Chaudhari, Struct. Chem. 23 (2012) 637.
[24] B.J. Hathaway, D.G. Holah, J. Chem. Soc. 0 (1964) 2408.
[25] S.O. Kim, C.V. Sastri, M.S. Seo, J. Kim, W. Nam, J. Am. Chem. Soc. 127 (2005) 4178.
[26] Heterogeneous Catalysis, American Chemical Society, 1983.
[27] T. Mallat, A. Baiker, Chem. Rev. 104 (2004) 3037.
[28] Z. Shi, C. Zhang, C. Tang, N. Jiao, Chem. Soc. Rev. 41 (2012) 3381.

Please cite this article in press as: R. Li, et al., Dioxygen activation at room temperature during controllable and highly efficient acetaldehyde-to-acetic acid oxidation using a simple iron(III)–acetonitrile complex, Catal. Today (2013), http://dx.doi.org/10.1016/j.cattod.2013.09.036